CSIRO PUBLISHING

www.publish.csiro.au/journals/ijwf *International Journal of Wildland Fire* **2009**, *18*, 711–721

An inverse method to estimate stem surface heat flux in wildland fires

Anthony S. Bova[A,B] *and Matthew B. Dickinson*[A]

[A]Forest Service, US Department of Agriculture, Northern Research Station, 359 Main Road, Delaware, OH 43015, USA.

[B]Corresponding author. Email: abova@fs.fed.us

Abstract. Models of wildland fire-induced stem heating and tissue necrosis require accurate estimates of inward heat flux at the bark surface. Thermocouple probes or heat flux sensors placed at a stem surface do not mimic the thermal response of tree bark to flames. We show that data from thin thermocouple probes inserted just below the bark can be used, by means of a one-dimensional inverse heat conduction method, to estimate net heat flux (inward minus outward heat flow) and temperature at the bark surface. Further, we estimate outward heat flux from emitted water vapor and bark surface re-radiation. Estimates of surface heat flux and temperature made by the inverse method confirm that surface-mounted heat flux sensors and thermocouple probes overestimate surface heat flux and temperature. As a demonstration of the utility of the method, we characterized uneven stem heating, due to leeward, flame-driven vortices, in a prescribed surface fire. Advantages of using an inverse method include lower cost, ease of multipoint measurements and negligible effects on the target stem. Drawbacks of the simple inverse model described herein include inability to estimate heat flux in very moist bark and uncertainty in estimates when extensive charring occurs.

Additional keywords: heat transfer, mass flux, modeling.

Introduction

Accurate estimates of inward heat flux or temperature at the surface of stems are necessary to validate models of heat transfer and tissue necrosis resulting from wildland fires. Such models use data from, typically, Schmidt–Boelter-type heat flux sensors (HFS) or thermocouple probes (TCP) mounted at the surface of tree boles exposed to flames (van Mantgem and Schwartz 2003; Jones *et al*. 2004, 2006; Bova and Dickinson 2005). These instruments, however, do not mimic the thermal response of tree bark to convective or radiant energy because their thermophysical properties differ from those of bark. Nor do they account for the energy lost owing to evaporation of water or escape of volatiles at the bark surface; thus, net heat flux (i.e. inward minus outward energy flow) is overestimated. These disparities may lead to inaccurate estimates of temperature or heat flux boundary conditions in physical models of heat transfer and fire effects.

An alternative approach is to estimate the surface (boundary) conditions from temperature changes within the bark during heating. In the case of a known boundary condition, such as surface heat flux, the temperature–time profile of heated material can be modeled accurately by analytical or numerical methods. The reverse of this process, estimating unknown surface heat flux from an internal temperature–time profile, is known as the inverse heat conduction problem (IHCP). Such inverse problems are usually ill-posed mathematically, rendering solutions unstable and therefore difficult to solve (Groetsch 1993).

Numerous methods of varying complexity have been applied to versions of this problem. The maximum entropy method (MEM) seeks a unique solution to the IHCP by maximizing an entropy functional, though total transferred energy (i.e. time-integrated net heat flux) must be approximately estimated by another technique before this method can be applied (Kim and Lee 2002). In the sequential function specification method (SFSM), some functional form (constant, linear, parabolic, etc.) of surface heat flux is assumed to apply between time steps (Beck *et al*. 1996; Lin *et al*. 2004). Other approaches utilize Newton's method (Dorai and Tortorelli 1997), the Laplace transform technique (Monde *et al*. 2003), singular value decomposition of an operator matrix (Shenefelt *et al*. 2002; Lagier *et al*. 2004), the boundary element method (Lesnic *et al*. 1996) and the conjugate gradient method (Huang and Yeh 2002). These citations are only examples, as the literature on these methods and others is extensive.

We chose the method of Tikhonov regularization, in which an approximation of a least-squares solution is obtained by the addition of a positive smoothing parameter to a vector operator (Groetsch 1993). The method is outlined in some detail below.

In the present paper, we present the results of laboratory experiments in which the above IHC (inverse heat conduction) method was tested. Further, we compare estimates of net surface heat flux and temperature with measurements made by Schmidt–Boelter-type HFS and surface-mounted TCPs respectively. Finally, we report the results of a field test of the method.

Heat transfer to a stem or bole in a surface fire

Net heat flux at a bole or stem surface is determined by several factors. A surface fire transfers heat to a tree bole by thermal radiation and, when flames or heated gases move over the bole,

 10.1071/WF07122 1049-8001/09/060711

by convection. The amount of incident thermal radiation that is absorbed depends on the reflectance (the fraction of incident radiation reflected) of its bark. Bark reflectance is variable among and between species, with values ranging from 0.1 to as high as 0.7 in the near- and shortwave-infrared range (Radeloff *et al*. 1999; Kötz *et al*. 2004; Roberts *et al*. 2004). A bole will emit thermal radiation in proportion to the fourth power of its absolute temperature, thus reducing net heat flux.

Convective heat transfer to or from a stem is governed by the temperature difference between surrounding gases and the stem, i.e. $q''_{\text{convection}} = h(T_{\text{gas}} - T_{\text{stem}})$. The coefficient of proportionality, h, is a function of the velocity and physical properties of the flowing gas, as well as physical properties and surface features of bark. The bole will lose heat by convection if its temperature is greater than that of surrounding air or gases, and by evaporated water, gases and volatiles that escape through the bark surface.

These factors may be combined to give the approximate heat balance relation at the surface of a small control volume of the bole that includes the bark:

$$q''_{\text{radiation(incident)}} - q''_{\text{radiation(emitted+reflected)}} + q''_{\text{convection}} - q''_{\text{mass(out)}} = q''_{\text{net}} \quad (1)$$

For simplicity, we have not included a term for heat generated at or below the bark surface (e.g. by smoldering combustion), and the energy lost by emitted water, gases and volatiles has been combined into the last term on the left-hand side. Note that net heat flux may be negative if the surface loses more heat than it absorbs, for instance, during cooling.

A TCP inserted below the bark surface responds to heat energy conducted by the bark. Radial conduction of heat within bark *near the surface* can be modeled in one dimension if it is assumed that bark is a homogeneous, semi-infinite solid with constant thermal diffusivity and that heating is uniform, at any given moment, over a small region of the bark surface normal to a given radius (Dickinson and Johnson 2001). Also assuming that no internal heat is generated, conduction may be expressed by the following one-dimensional heat-transfer equation (see *Nomenclature* section below for definitions of symbols and variables):

$$\frac{\partial^2 T}{\partial x^2} = \frac{1}{\alpha}\frac{\partial T}{\partial t} \quad \text{(Incropera and DeWitt 2002)} \quad (2)$$

subject to the boundary conditions

$$q''_0 = -k\frac{\partial T}{\partial x} \quad (x = 0, 0 \le t \le t_{\max}) \quad (3)$$

$$\frac{\partial T}{\partial t} = 0 \quad (x = L, 0 \le t \le t_{\max}) \quad (4)$$

and the initial condition

$$T = 0 \quad (0 \le x \le L, t = 0) \quad (5)$$

Given a constant heat flux, q''_0, at the surface ($x = 0$), the solution to Eqn 2 is:

$$T(x, t) = \frac{2q''_0(\alpha t/\pi)^{1/2}}{k}\exp\left(\frac{-x^2}{4\alpha t}\right) - \frac{q''_0 x}{k}\text{erfc}\left(\frac{x}{2\sqrt{\alpha t}}\right) \quad (6)$$

where erfc is the complementary error function (Carslaw and Jaeger 2003).

The inverse heat conduction problem

Inverse problems may be informally described as those in which causes are estimated from effects. As originally defined by the mathematician Jacques Hadamard, a well-posed mathematical problem must have a solution that exists, is unique, and is stable with respect to perturbations (Kurpisz and Nowak 1995). Inverse physical problems are usually ill-posed in that their solutions may not exist, or, if they do, may not be unique or depend continuously on data (Engl *et al*. 1996).

In the case of heat conduction, this may be understood intuitively. Temperature fluctuations at the surface of a solid are quickly damped and smoothed as heat energy propagates inward, especially in low-diffusivity materials such as bark. Thus, small temperature fluctuations below the surface correspond to large fluctuations at the surface, making an inverse estimate extremely sensitive to noise in the measurements. In addition, there is often a significant time lag between changes in surface temperature and resulting changes below the surface. The result is that, to make an inverse estimate of a surface condition at a given time, internal temperature data beyond that time are required. For a more detailed discussion of these points, see Kurpisz and Nowak (1995, ch. 1).

By Duhamel's principle, a solution in the case of transient surface heat flux may be written as:

$$\theta(x, t) = \int_0^t q''(0, \lambda)\frac{\partial T(x, t-\lambda)}{\partial t}d\lambda \quad (7)$$

where T in this case is the solution to the constant heat flux function (Eqn 6) (Carslaw and Jaeger 2003). At a given, discrete point (i.e. a node) below a surface, Eqn 7 can be approximated in matrix form as:

$$\mathbf{D}\mathbf{q}_0 = \boldsymbol{\theta} \quad (8)$$

where the sensitivity operator, $\mathbf{D}$, is a lower-triangular matrix of coefficients:

$$\mathbf{D} = \begin{bmatrix} 0 & & & & \\ d_1 & 0 & & & \\ d_2 & d_1 & 0 & & \\ \vdots & \ddots & \ddots & \ddots & \\ d_n & \cdots & d_2 & d_1 & 0 \end{bmatrix} \quad (9)$$

and each element, d_j, is the rate of temperature change between time index j and $j+1$ at the given node in response to a unit heat flux pulse. In other words, each element of $\mathbf{D}$ is a discrete approximation of the partial derivative in Eqn 7 for $q''(0, t) = 1$, where the units of q'' are arbitrary (Alifanov 1994).

In most IHCPs, there is no inverse solution to Eqn 8 in the traditional form (i.e. $\mathbf{q}_0 = \mathbf{D}^{-1}\boldsymbol{\theta}$) because $\mathbf{D}$ is singular. The inverse solution can be approximated, however, by modifying the traditional form with a regularization parameter, β, where $\beta > 0$. Eqn 8 then takes the regularized form $(\mathbf{D}^{\mathrm{T}}\mathbf{D} + \beta\mathbf{I})\mathbf{q}_0 = \mathbf{D}^{\mathrm{T}}\boldsymbol{\theta}$. The operator in parentheses may be inverted; thus it can be solved to give an approximation of the surface heat flux vector. Assuming now that $\boldsymbol{\theta}$ is a vector of measured temperatures at a known depth, the approximated surface heat flux is given by:

$$\mathbf{q}_0 = (\mathbf{D}^{\mathrm{T}}\mathbf{D} + \beta\mathbf{I})^{-1}\mathbf{D}^{\mathrm{T}}\boldsymbol{\theta} \quad (10)$$

This equation is known as the Tikhonov approximation to $\mathbf{q}_0 = \mathbf{D}^{-1}\boldsymbol{\theta}$ (Groetsch 1993). Although we focus here on estimating net surface heat flux, direct inverse estimates of surface temperature are also possible.

Finding a value of the regularization parameter that gives the best approximation of Eqn 8 is not trivial. A value that is too high will greatly dampen the solution, resulting in a highly smoothed curve that only vaguely resembles the actual heat flux profile. Values that are too low will produce a very noisy solution, or not provide enough conditioning to render the operator in the regularized equation invertible.

We chose the popular L-curve method to find an appropriate value for the regularization parameter (Hansen 2001). If $\mathbf{q}_\beta$ represents a solution vector based on a particular regularization parameter, then a parametric plot, over a range of values of β, of the norms, $\|\mathbf{q}_\beta\|$, against the residual norms $\|\mathbf{D}\mathbf{q}_\beta - \boldsymbol{\theta}_0\|$ on a log-log or semi-log scale usually results in a characteristic L-shaped curve (see *Results*). The value of β corresponding to the corner of this curve represents a compromise between error resulting from too much damping (regularization) and error from the data. Wu (2003) suggests plotting $\ln(1/\beta)$ against $\|\mathbf{q}_\beta\|$, which works at least as well as the former method. The corner-point of the L-curve can be chosen by visual examination, though algorithms exist to determine the corner point numerically (e.g. Castellanos *et al*. 2002).

Methods

Laboratory experiments

One-metre sections of red oak (*Quercus rubrum*), white ash (*Fraxinus americana*) and black locust (*Robinia pseudoacacia*) boles were cut in wooded areas in Delaware county, Ohio, USA. The sections ranged from 6 to 8 cm in diameter. In the laboratory, three small cross-sections, roughly 4 cm long, were cut from each 1-m bole section. Each of the smaller sections was measured and the sawn ends sealed with paraffin to prevent moisture loss through vessels during heating. Five bark samples (~0.2 to 1 g) were chiseled from the remaining portion of each bole section and weighed. Three bark samples were dried at a constant temperature of 103°C until weights no longer changed. The final weight was used to estimate average moisture content on a dry weight basis. The remaining sample pairs of bark were prepared in order to estimate specific gravity by the buoyant force method (Siau 1995). The specific gravity of bark is defined as dry mass divided by volume at the original moisture content (Martin 1963; Siau 1995). The values of specific gravity used in the estimates below were 0.79, 0.52 and 0.29, for oak, ash and locust respectively. The dimensionless porosity (i.e. void fraction) of each bark sample was estimated based on its specific gravity according to Siau (1995).

Using a high-speed handheld rotary tool (Dremel-Robert Bosch Tool Corp., Mount Prospect, IL) with a 1.16-mm diameter bit, two small pilot holes were drilled through a sawn end longitudinally and parallel with the bark surface into the dead bark. The holes were ~2 cm long, 1 to 4 mm below the bark surface, and separated by 1 to 2 cm (Fig. 1). After drilling, each cross-section was weighed on a microbalance (sensitivity and s.d. = 0.001 g).

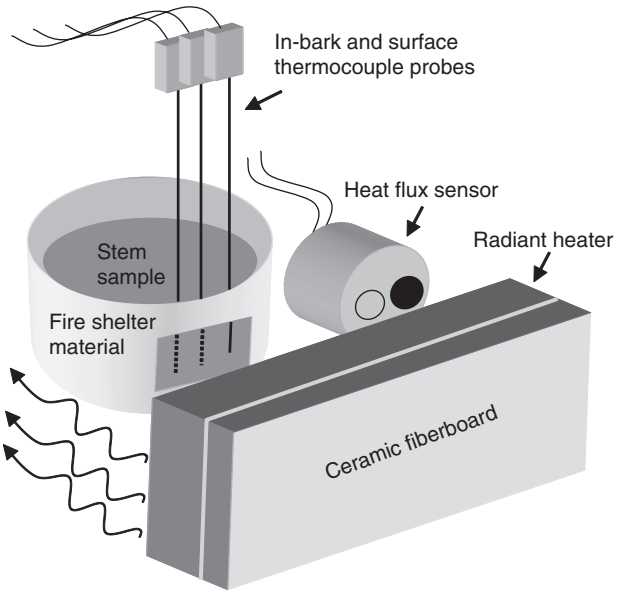

Fig. 1. Configuration of radiative heating experiments.

Two 0.52-mm diameter, 15-cm long, type K TCPs were inserted as far as possible into the pilot holes. According to the manufacturer (Omega Engineering, Inc., Stamford, CT), the error in indicated temperature is less than 2.2°C (or 0.75%, whichever is greater) over the temperature range 0 to 1250°C. The TCPs have AISI 304 stainless steel jackets and ungrounded thermocouple junctions. A third TCP of the same type was placed so that its tip was in contact with the bark surface (Fig. 1).

In each trial, a cross-section was masked with fire shelter material (reflectance ≈ 0.95) cut so that a small window (2.5 × 3 cm) would allow bark to be exposed to radiant heat. The mask extended 2 cm above the top of the stem cross-section so that the exposed portions of the TCPs near the insertion points were shielded from thermal radiation (Fig. 1).

A Schmidt–Boelter-type HFS (Medtherm Corporation, Huntsville, AL) was placed ~2 cm from one side of the cross-section so that its face was parallel with the bark surface exposed in the mask window (Fig. 1). The HFS contains two transducers that indicate total (convective plus radiative) and radiative heat flux at the sensor surface. The radiation transducer is the same as the convective, except that it is covered by a sapphire window that allows the transmission of only thermal radiation. Because incident heat energy was only radiative, and because the sapphire window reflects 15% of incoming thermal radiation (from Medtherm brochure), data from only the total flux sensor were used. The body of the HFS is a relatively heavy (~120 g) copper cylinder 2.5 cm in diameter and 2.5 cm long. HFS and TCP leads were connected to a CR-10X data logger (Campbell Scientific, Inc., Logan, UT). Data were sampled at 1-s intervals.

The core of an electric room heater (5 cm in width, 16 cm in length and 2.8 cm deep), containing two layers of 4-cm wire elements spaced 0.25 cm apart, was mounted on 1.5-cm thick ceramic fiberboard (Cotronics Corp., Brooklyn, NY) to provide a source of radiant heat (Fig. 1). It was powered by a 120/140 V variable AC transformer (variac) (Staco Energy

Products, Dayton, OH), allowing adjustment of the maximum temperature and therefore the radiative power output. The heater core assembly was positioned to face the cross-section and HFS (Fig. 1). The heater face was 3 cm from the bark surface and the HFS. Uniformity of the heating area at that distance was tested by examining the scorch mark left by the heater on a panel of dry pine lumber. The mark uniformly darkened over an elongated elliptical area with major and minor axes of approximately the same length and width respectively as the heater. The darkened area faded over a short distance from its boundary. Because the window of the fire shelter material fit well within the uniformly scorched area, it was assumed that the panel provided uniform radiant heat over the enclosed area. In addition, TCP tips were positioned as near as possible to the centerline of the window so as to avoid edge effects. The HFS was also placed along the major axis of the darkened oval so that it was within the zone of uniform heating. A clamp-on ammeter was used to measure current levels across the heater core at several voltages in order to estimate power consumption.

In each trial, the variac was set to a predetermined level of 50, 60 or 70% of maximum (120 V). The heater core was allowed to heat for ~1 min to a roughly steady temperature while a large square of ceramic fiberboard, covered with fire shelter material, was placed in front of the heater to ensure that no thermal radiation was received at the bole section surface. The square was then removed, and the stem section allowed to heat for 90 s before the fiberboard was replaced and the transformer turned off. Data were recorded for an additional 60 s as the stem section cooled. After this period, the mask and TCPs were removed and the cross-section reweighed to measure mass loss during heating.

Shen *et al*. (2007) found that, when the temperature of wood heated by thermal radiation was less than 320°C, the evolved gases were primarily composed of water vapor and carbon dioxide. Therefore heat loss by mass transfer was estimated based on the assumption that most of the emitted mass was water vapor and that it was lost at a constant rate during heating (see *Discussion*). Below fiber saturation point (FSP ≈ 30% moisture content on dry weight basis), greater energy is needed to evaporate water bound in the cell walls of wood and bark. A polynomial correlation was therefore used to estimate the evaporation enthalpy based on initial moisture content (Galgano and Di Blasi 2004). Heat flux due to mass loss was estimated by multiplying the rate of mass loss by evaporation enthalpy and dividing the result by the area of the mask window (7.5 cm^2).

Heat loss by surface radiation was estimated assuming bark emissivity of 0.94, though this may be slightly lower than emissivity in the infrared range (Rubio *et al*. 1997).

Field tests

Shortly before a prescribed surface burn (~50 acres, ~20.2 ha) in the Racoon Ecological Management Area in south-eastern Ohio, a mature red oak (*Quercus rubra*) (35 cm diameter at breast height (DBH)) was selected and equipped as follows (Fig. 2). Five TCPs were inserted below the bark surface, spaced regularly around the bole (roughly 72° apart), ~20 cm above the mineral soil. In this test only, the bark surfaces above the inserted TCPs were shaved slightly with a razor to ensure a flat surface. As in the laboratory experiments, pilot holes were drilled with the handheld rotary tool. Each in-bark TCP was paired with a TCP positioned so that its tip was in contact with the bark surface and within 2 cm of the radial epicenter of the in-bark TCP. The exposed portion and plastic base of the TCPs were covered with a 10-cm square of ceramic fleece and fire shelter material. Inconel-wrapped, silica-insulated leads connected each set (five in-bark and five surface TCPs) to a separate CR10X data logger suspended by wire ~2 m above the litter bed (Fig. 2). Loggers and power supplies were placed in (14 × 28 × 17.5 cm) ammunition cans that were further insulated with blankets of ceramic fleece and covered with fire shelter material. Bark moisture was estimated based on the moisture of electronic 10-h fuel sticks at nearby locations.

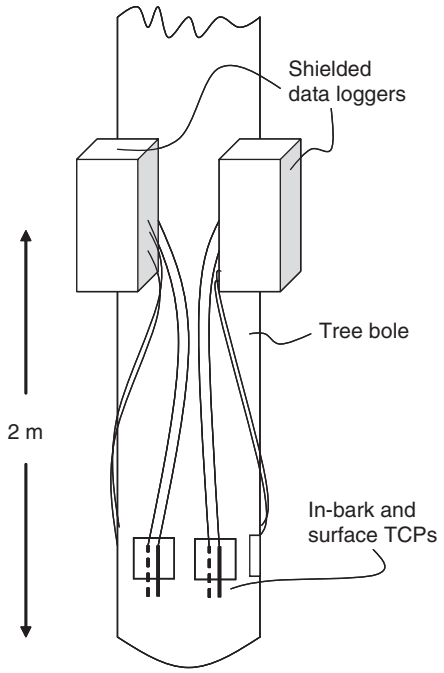

Fig. 2. Configuration of field test for uneven bole heating. TCP, thermocouple probe.

Field data were also taken from two 'wick fires', in which a length of fuel-soaked rope was wrapped around a bole and ignited. The boles were implanted with a heat flux sensor, face flush with the bark surface, and in-bark TCPs. The burns occurred in the spring and fall of 2002. For further details, see Bova and Dickinson (2005).

The inverse algorithm

The inverse algorithm was implemented in *Mathcad Professional 2001i* (Parametric Technology Corporation, Needham, MA). A general outline of the inverse procedure follows.

The time step, distance between spatial nodes and maximum size of the spatial domain are selected (1 s, 0.05 mm and 20 mm respectively in these tests). An estimate of the thermal conductivity and specific heat of bark, based on moisture content and specific gravity, is made using Martin's equations (Martin 1963). A temperature–time profile in response to a unit heat flux (1 kW m^{-2}) is then estimated, using Eqn 6, for all nodes in the spatial domain and at all time steps up to the maximum time.

An estimate of the in-bark TCP depth is entered and the estimated temperature–time profile (i.e. unit heat flux response) of the spatial node corresponding to this depth is used to build the sensitivity operator, **D** (Eqn 9). Separate estimates of surface heat flux, each corresponding to a different value of the regularization parameter, are generated according to Eqn 10. Twenty values of the regularization parameter, ranging from 1.9×10^{-6} to unity (where each value is twice the preceding value), were applied in these tests. Solution norms were plotted against the residual norms and an appropriate value of β was chosen from the resulting L-curve (see *Results*). Temperature profiles (i.e. the vectors **θ**) were then calculated for all nodes by Eqn 8. If, on visual inspection, the initial rise (over ambient) of estimated bark surface temperature did not temporally match the initial rise of the surface TCP, a new depth was guessed and the procedure repeated until they did. In field experiments, the temperature–time profiles of the surface TCPs and IHC surface temperature estimates contained many peaks and valleys; thus the TCP depth was adjusted until there was a temporal match between the profiles.

Test of algorithm and sensitivity

A mathematically generated surface flux comprising a square and triangle wave (Fig. 3) was used to test the above algorithm. The discontinuities (sharp corners) of these shapes provide a severe test of inverse estimates (Lesnic *et al*. 1996). Corresponding temperature profiles at all spatial nodes were generated by a finite difference algorithm using thermophysical properties of black locust, which had the lowest thermal diffusivity of the selected species, with a moisture content of 20% and density of $400\,kg\,m^{-3}$. The resulting temperature profile of the node corresponding to a depth of 2 mm was taken to be the 'TCP temperature'. The inverse algorithm was then tested at moisture contents, specific gravities and TCP depths ranging from +5 to −5% of the given values. The resulting flux estimates were reapplied to the finite difference routine, using original thermophysical values, to find the departures from the original values of maximum heat flux, time-integrated heat flux, and maximum temperature at the 2-mm depth.

Results

Sensitivity tests

The inverse estimates of heat flux in Fig. 3 show rounding of corners and smoothing of peaks that increase with depth. This is typical of inverse estimates regardless of method. Despite this smoothing, the corresponding regenerated surface temperature profiles are very similar to the original profile. In the inverse estimate, the greatest departures from the values of the prescribed heat flux function and calculated temperature profile occurred when the specific gravity, bark moisture and TCP depth parameters were all at the same prescribed limit of error (i.e. the exact value ±5%). With these parameters all at either their lowest or highest error values, peak heat fluxes differed from exact values by −16 or 8% respectively; estimated peak temperatures at the target depth (2 mm) differed by 1 or −1%; and time-integrated heat flux differed by −9 or 11%.

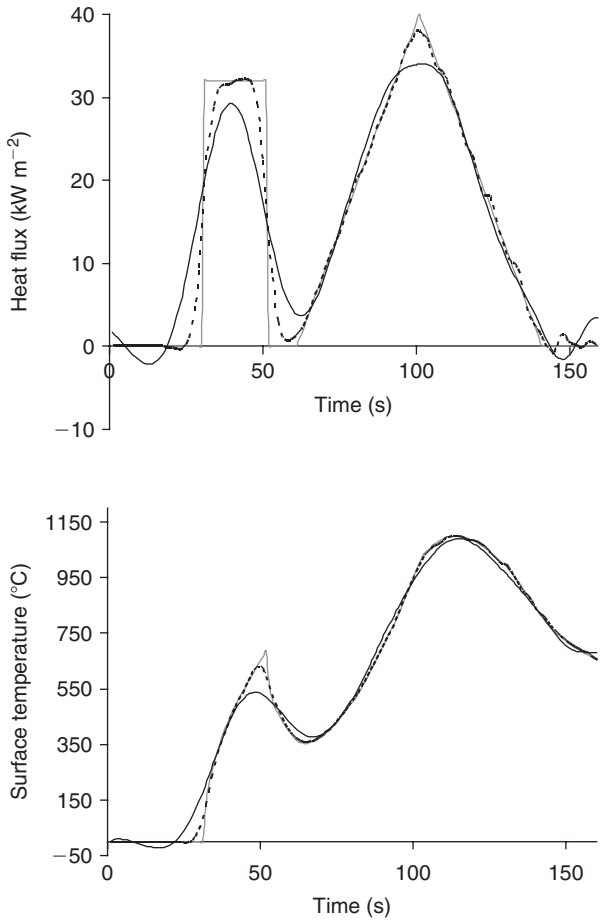

Fig. 3. Sensitivity test plots. Solid gray lines are the prescribed heat flux function (top) and resulting surface temperature (bottom). Dotted and solid black lines indicate inverse estimates at 1- and 5-mm depths respectively.

Laboratory experiments

Examples of inverse estimates and modeled temperatures from bole samples heated by thermal radiation are shown in Fig. 4. Inverse estimates of inward heat flux were significantly lower than heat flux measured by the HFS (Table 1). When outward heat flux from evaporation and surface radiation (Eqn 1) were added to the net flux, however, the resulting estimates were closer to the HFS values (Table 1 and Fig. 4). Note that mean estimated outward fluxes from evaporation were simply added to the net fluxes for the purpose of visual comparison in Fig. 4; thus the thin solid lines in the figure do not necessarily represent the exact sum of fluxes at a given time.

Grouping all species, energy lost by evaporation (outward mass flux multiplied by evaporation enthalpy – see *Methods*) showed a positive linear correlation to the intensity of incident radiation as measured by the HFS ($R^2 = 0.58$, $n = 9$, s.e. $= 1.52\,kW\,m^{-2}$), though each species responded differently. For all species, roughly 1/3 of incident energy was lost as evaporation. Evaporative energy flux correlated considerably better, however, to the intensity of incident radiation normalized by (i.e. multiplied by) estimated bark porosity (Fig. 5). The constant of the linear regression ($0.61\,kW\,m^{-2}$) was not significant at the 5%

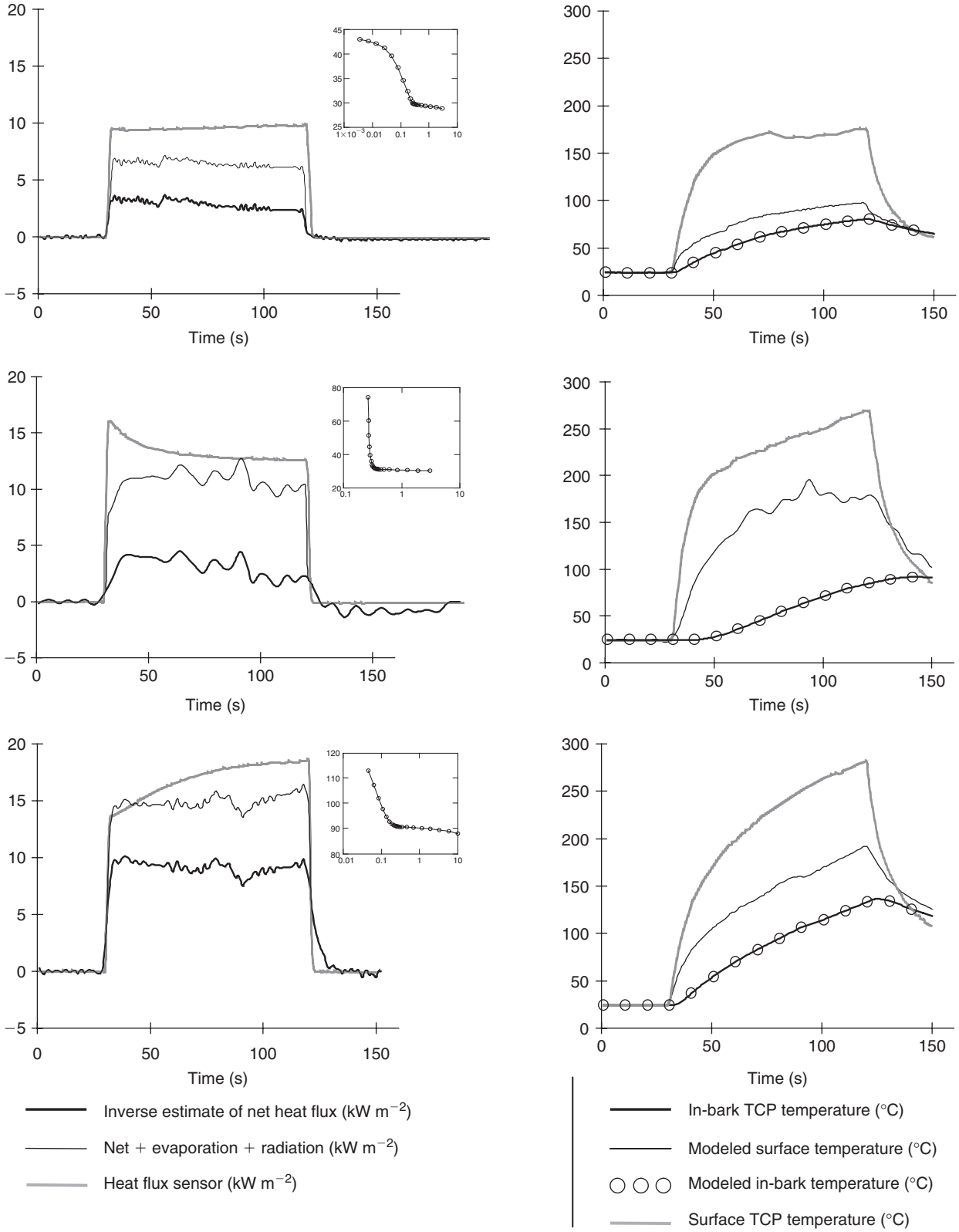

Fig. 4. Selected plots of heat fluxes and surface temperatures estimated by inverse method compared with corresponding data from sensors. Inset images are L-plots used to select smoothing parameter. TCP, thermocouple probe.

Table 1. Results from samples heated by thermal radiation and wick fire tests
See list in the *Nomenclature* section for definition of abbreviations

Species or burn number	Estimated TCP depth (mm)	Regularization parameter (dimensionless)	HFS mean flux ($kW\,m^{-2}$)	s.d.	IHC estimated mean net flux ($kW\,m^{-2}$)	s.d.	IHC mean estimated total flux ($kW\,m^{-2}$)	Surface TCP max. (°C)	IHC estimated bark surface max. (°C)
White ash	1.1	7.81×10^{-3}	9.6	0.1	2.8	0.5	5.6	176	98
White ash	2.5	2.44×10^{-4}	14.7	1.1	4.1	1.2	8.6	217	149
White ash	2.1	2.44×10^{-4}	20.6	2.5	4.8	2.0	11.1	257	146
Black locust	5.0	9.77×10^{-4}	7.9	0.8	2.2	1.1	5.2	169	153
Black locust	3.5	9.77×10^{-4}	13.3	1.0	3.0	0.9	8.9	270	214
Black locust	2.6	1.95×10^{-3}	18.3	0.4	3.5	0.6	13.1	488	210
Red oak	0.8	3.10×10^{-2}	7.1	0.1	4.9	0.5	6.6	136	113
Red oak	1.7	4.88×10^{-4}	13.0	0.4	7.2	2.4	10.1	226	138
Red oak	1.6	1.95×10^{-3}	16.7	2.2	9.0	0.8	13.0	281	192
Wick 31	2.8	4.88×10^{-4}	20.5	11.6	7.2	1.80	11.1	–	128
Wick 33	2.4	4.88×10^{-4}	25.5	13.4	7.1	3.00	11.7	–	131

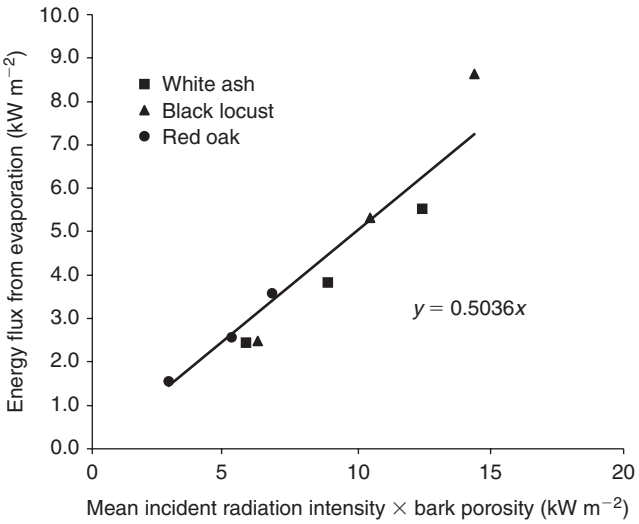

Fig. 5. Energy lost by evaporation (mass flux) of samples exposed to thermal radiation plotted against incident radiation intensity multiplied by estimated bark porosity. It was assumed that all emitted mass was water vapor.

level; thus the regression line has been forced through the origin. Interpreting the R^2 value of such a regression line is problematic (Eisenhauer 2003), but the R^2 value of the original equation was 0.92 ($n = 9$, s.e. $= 0.66\,kW\,m^{-2}$).

Bark surface temperatures estimated by the IHC algorithm were lower than those of the TCPs in contact with the bark surfaces, though the shape of the estimated profiles generally matched those of the surface TCPs (Fig. 4). Peak estimated bark surface temperatures averaged ~70% of the peak surface TCP temperatures (Table 1).

Field experiments

Flame lengths were ~1 m near the instrumented bole. The lowest and highest positive net fluxes corresponded to the windward and leeward sides of the bole respectively (Fig. 6). Estimated peak bark surface temperatures were approximately half of the peak surface TCP temperatures (Table 2).

In-bark TCP data from two wick fires (see *Methods*) were also used to make inverse heat flux estimates. Unlike the previous cases, there were no surface-mounted TCPs, but rather an HFS mounted so that its face was flush with the bark surface. TCP depth was estimated by matching the shape of the inverse heat flux profile with that of the HFS (Fig. 7). An interesting feature of such fires is that the flames are optically thin; thus heat transfer is mostly by convection rather than radiation as in the laboratory tests. Although there were no mass loss data for the wick fires, mass flux was estimated from the correlation shown in Fig. 5 by assuming that the total flux indicated by the HFS was the true incident flux (see *Discussion*). Estimated net flux plus estimated evaporative and radiative outfluxes are shown in Fig. 7.

Discussion

Given the inherent uncertainty of inverse estimates, it is encouraging that the inverse algorithm generated inward heat flux

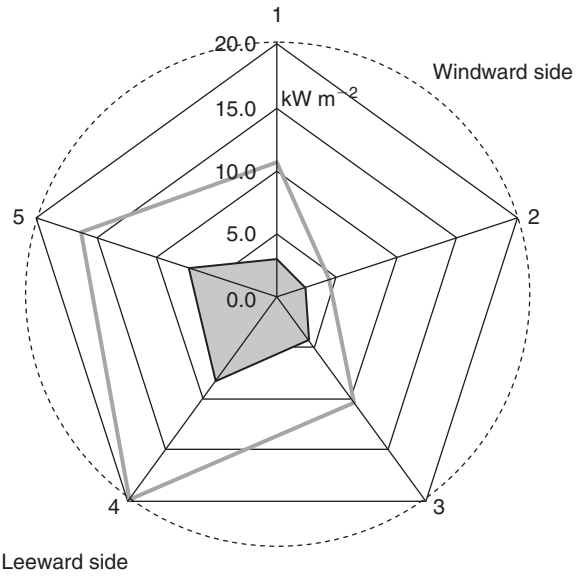

Fig. 6. Radial plot of 1-min average (solid gray) and peak (gray line) heat fluxes around a tree bole in uneven heating field test. A standing flame caused higher heat flux on the leeward side of the tree.

profiles with features that temporally matched those of the corresponding HFS profiles. The differences between estimated net heat fluxes and the fluxes measured by the HFS were significant (Table 1). Sensitivity tests indicate that, unless the thermophysical properties of the various barks were grossly misestimated, the differences are likely to be real. We assume here that the HFS gives an accurate measure of incident thermal radiation, though uncertainties in incident radiative flux of 7 to 29% have been estimated for such sensors (Bryant *et al*. 2003).

The disparity between heat flux as indicated by the HFS, and as estimated by the inverse method is especially pronounced in the wick fire tests (Fig. 7). This was not unexpected as, owing to its heat capacity and high thermal diffusivity, the copper body of the HFS is most likely cooler than the bark surface. Thus, *ceteris paribus*, the HFS experiences greater convective heat transfer than the nearby bark. As mentioned, thermal radiation emittance was very low in these particular tests owing to the thin flames, so convection was the dominant mode of heat transfer. Energy loss by evaporation was estimated by assuming that the flux indicated by the HFS was the true intensity of incident energy at the bark surface; thus it is probably overestimated in Fig. 7.

The differences between maximum temperatures of the surface-mounted TCPs and estimated maximum bark temperatures are probably the result of several factors. The AISI 304 stainless steel jackets of the TCPs have lower emissivity ($\approx$0.2, Gardner and Ng 2006) than bark; thus, they radiate less energy than bark at a given temperature. Also, unlike TCPs, heated bark loses energy through emitted mass, lowering the rate of temperature increase. Last, a portion of the tip is, in effect, insulated by the less conductive bark with which it is in contact, thus reducing its ability to lose heat.

Although the time-course of mass loss was not measured during heating in the laboratory experiments, prior laboratory tests for mass loss, in which the time-course of stem sample weight was measured during radiative heating, indicate that it begins within a few seconds after the incidence of thermal radiation (A. S. Bova and M. B. Dickinson, unpubl. data). The rate of loss was constant over the relatively short time of heating ($\sim$90 s), with a value proportional to the intensity of incident radiation, and diminished rapidly after the cessation of heating. However, Shen *et al*. (2007) found that the rate of mass loss of wood samples increased over the course of longer periods of heating ($\sim$500 s) at constant incident radiation intensities.

Energy lost through evaporation seems to be mostly a function of incident energy intensity and porosity, at least over short heating times (Fig. 5). Note that we refer to the *intensity* of incident radiation rather than the *flux* to avoid the implication that all incident thermal radiation flows through the bark surface (i.e. is unreflected). It was assumed that the flux of incident thermal radiation to the highly absorptive sensor portion of an HFS, however, was an accurate measure of incident thermal radiation. It is possible that the evaporation relation shown in Fig. 5 would also hold when heating is convective, though this was not tested. As mentioned, convective flux to an HFS may not be the same as that to nearby bark. Without direct measurement, however, gas (or flame) temperature and velocity, as well as bark surface temperature, are needed to estimate convective flux, making testing more difficult.

The field test showing uneven heating of the bole (Fig. 6) suggests that an inverse method is well suited for studying this phenomenon. In surface fires, tree boles are often heated more on the leeward side owing to the formation of vortices that increase flame length and residence time (Gutsell and Johnson 1996). To monitor this effect, accurate multipoint heat flux data would be ideal. A tree bole could be instrumented with more than 30 TCPs ($\sim$US$35 per unit), located at various heights and circumferential positions, for the same cost as one HFS ($\sim$US$1200 per unit). Infrared imaging, though expensive, would be useful for describing leeward heating and in validating inverse estimates and models of leeward heating.

Sources of error

It is assumed that, unlike TCPs at the bark surface, TCPs inserted below the bark surface indicated the true temperature of the bark (within the accuracy of the TCPs and data logger; see *Methods*). This is reasonable given that the thin TCPs used in these tests have rapid response times and because their tips were in tight contact with the bark that surrounded them.

It is difficult to accurately measure the depth of a TCP tip below the bark surface. The bark of all three species used in these experiments can be deeply furrowed, especially with growth and aging. The outer bark of white ash, in particular, develops a somewhat regular checkered pattern and may be considered the roughest of the three species. The depth of furrows measured on a bole section that was 8 cm in diameter ranged from 2 to 5 mm. In the case of one-dimensional approximation, it is not trivial to define a depth below the non-ideal, three-dimensional surface of bark. We chose to address this by placing a TCP in contact with the bark surface (see *Methods*). Although it was not expected to provide the true bark surface temperature, the surface TCP provided a reference for the beginning of heating and the rough shape of the surface temperature profile. In the inverse

Table 2. Field data showing uneven stem heating (see also Fig. 6)

TCP	Estimated TCP depth (mm)	Regularization parameter (dimensionless)	IHC 60-s mean inward flux ($kW\,m^{-2}$)	s.d.	IHC maximum ($kW\,m^{-2}$)	Surface TCP max. (°C)	IHC estimated surface max. (°C)
0	1.5	1.90×10^{-3}	3.0	2.5	10.6	183	92
1	1.2	3.10×10^{-2}	2.4	0.8	4.4	151	67
2	0.8	1.90×10^{-3}	4.3	2.0	10.4	252	114
3	0.6	7.80×10^{-3}	8.2	5.9	19.8	309	210
4	0.8	3.90×10^{-3}	7.2	4.6	16.3	340	182

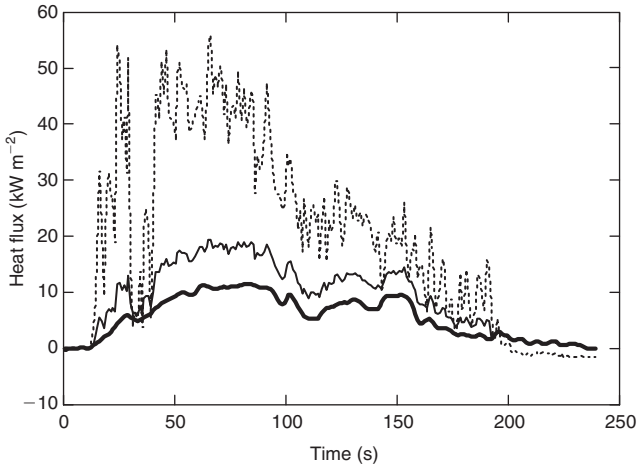

Fig. 7. Convective plus radiative heat flux indicated by heat flux sensors (HFS) (dotted line) and inverse estimate of net heat flux (solid line) in a wick fire. Net flux added to estimated emitted radiation and evaporation flux is indicated by the thin solid line. Incident radiative intensity, as indicated by the Schmidt–Boelter HFS, was very low (mean = $0.7\,kW\,m^{-2}$).

algorithm, the depth of the TCP is adjusted until features of the estimated surface temperature profile temporally match those of the surface TCP, especially near the beginning of heating.

Thermophysical properties of the bark were estimated from regression equations found in Martin (1963). Martin's equations are assumed to be representative because they characterize the pooled data from three pine and seven hardwood species. Margins of error were not specifically reported; however, the thermal conductivity relation used in the above model had an R^2 value of 0.981 when regressed against measured data (Martin 1963). As it relates to Eqn 2, Martin's most important finding was that thermal diffusivity, α, is roughly constant over a wide range of bark moistures and densities at temperatures from 0 to 100°C. In the inverse model, the estimated temperature profile (Eqn 6) depends on the thermophysical properties, which may mean that inaccuracies in the measured moisture content and specific gravity could lead to inaccuracies in the estimated TCP depth, and, therefore, net heat flux.

Sensitivity tests suggest, however, that when features of the estimated surface temperature and surface TCP temperature are temporally matched, the estimated TCP depth is accurate and the resulting error in estimated inward heat flux is roughly the same as the error in the thermophysical parameter estimates. In other words, a 10% error in the estimate of specific gravity leads to an error of ~10% in the estimate of total energy absorbed.

High moisture content may also lead to error in an inverse estimate. Bark moisture that is greater than FSP may cause the in-bark TCP temperature to plateau at ~100°C for an unspecified time. Because the inverse method relies on TCP temperature change to estimate flux, the constant temperature will be regarded as a state of thermal equilibrium and estimated inward flux will be zero even though considerable heat energy is being transferred into the bark surface. In typical prescribed burns, however, bark moisture will generally be lower than FSP.

Suggestions for further testing

Surface temperature estimates from the inverse method were generally lower than those of surface-mounted TCPs. In future experiments, independent means of measuring bark surface temperature, such as by infrared measurements, should therefore be used to test the method.

As mentioned in the introduction, the Tikhonov method used here is only one of many available for making inverse estimates of temperature and heat flux. It is possible that another method would give better results. An advantage of this method is that simply by changing the temperature function (Eqn 6), or by using results from finite element simulations, the sensitivity operator can be changed to account for different geometries or additional dimensions. A shortcoming of inverse heat conduction methods in general is that, unlike the HFS, they cannot distinguish between convective and radiative heat flux (Nakos 2005).

The transient heat flux solution (Eqn 7) requires that thermophysical properties be regarded as constant, though the thermal conductivity and heat capacity of bark increase with temperature (Martin 1963). In addition, changes in thermal conductivity due to char formation, and net heat flux variation due to endothermic processes such as pyrolysis and evaporation, were not considered in the model described above. For the relatively low heat fluxes and temperatures involved, these were probably not major sources of error. A more advanced model of stem or wood heating (e.g. Jones *et al*. 2004, or Shen *et al*. 2007 respectively) that accounts for these effects could be used to estimate the likely temperature field resulting from a given net heat flux. An inverse estimate of net heat flux may then be achieved by means of, for example, the so-called conjugate gradient method (Alifanov 1994). Inverse estimates of net heat flux, when subtracted from measurements of incident thermal radiation (or accurate estimates of convective heating), can be used to

check evaporation and re-radiation estimates given by advanced stem-heating models (e.g. Jones *et al*. 2006).

Conclusion

The ability to estimate inward heat flux is necessary for the validation of models of heat transfer to stems and of resulting effects on stem tissues. Results suggest that an inverse method provides realistic estimates of net heat flux to a stem surface, allowing estimates of moisture loss, re-radiation and surface temperature to be made. Measurements of total heat flux from HFS alone give biased estimates of bark surface conditions because convective heat flux is greater to Schmidt–Boelter-type HFS than to surrounding bark. In addition, temperatures indicated by surface-mounted TCPs exposed to flames are generally higher than the temperature of the bark they contact, owing in part to the low emissivity, relative to tree bark, of stainless steel-jacketed TCPs. Estimates of net heat flux may be combined with measurements of incident radiative flux from HFS, or from surface temperatures determined by infrared detectors, to improve and validate models of stem surface heat flux and fire effects.

Nomenclature

Upper- and lowercase characters

h, coefficient of convection ($W\,m^{-2}\,K^{-1}$);
k, coefficient of conduction ($W\,m^{-1}\,K^{-1}$);
L, limit of spatial region (m);
q, heat energy (J);
t, time (s);
T, temperature (K);
x, spatial coordinate (m).

Bold characters

$\mathbf{D}$, coefficient matrix;
$\mathbf{I}$, identity matrix;
$\mathbf{q}$, heat flux vector ($W\,m^{-2}$);
$\mathbf{T}$, temperature vector (K);
$\boldsymbol{\theta}$, measured temperature vector (K).

Greek symbols

α, thermal diffusivity ($m^2\,s^{-1}$);
β, regularization parameter (dimensionless);
θ, temperature vector.

Subscripts

$_i$, spatial node (dimensionless);
$_j$, temporal node (dimensionless);
$_0$, value at $x = 0$ (surface value).

Superscripts

$''$, per unit area;
^{T}, transpose of matrix;
$^{-1}$, inverse of matrix.

Acknowledgements

We thank laboratory technicians Kelley McDonald and Tess Schmaltz for their time, patience and attention to detail.

References

Alifanov OM (1994) 'Inverse Heat Transfer Problems.' (Springer-Verlag: New York)

Beck JV, Blackwell B, Haji-Sheikh A (1996) Comparison of some inverse heat conduction methods using experimental data. *International Journal of Heat and Mass Transfer* **39**, 3649–3657. doi:10.1016/0017-9310(96)00034-8

Bova AS, Dickinson MB (2005) Linking surface fire behavior, stem heating, and tissue necrosis. *Canadian Journal of Forest Research* **35**, 814–822. doi:10.1139/X05-004

Bryant R, Womeldorf C, Johnson E, Ohlemiller T (2003) Radiative heat flux measurement uncertainty. *Fire and Materials* **27**, 209–222. doi:10.1002/FAM.822

Carslaw HS, Jaeger JC (2003) 'Conduction of Heat in Solids.' 2nd edn. (Oxford University Press: Oxford, MA)

Castellanos JL, Gómez S, Guerra V (2002) The triangle method for finding the corner of the L-curve. *Applied Numerical Mathematics* **43**, 359–373. doi:10.1016/S0168-9274(01)00179-9

Dickinson MB, Johnson EA (2001) Fire effects on trees. In 'Forest Fires: Behaviour and Ecological Effects'. (Eds E Johnson, K Miyanishi) pp. 477–525. (Academic Press: San Diego, CA)

Dorai GA, Tortorelli DA (1997) Transient inverse heat conduction problem solutions via Newton's method. *International Journal of Heat and Mass Transfer* **40**, 4115–4127. doi:10.1016/S0017-9310(97)00044-6

Eisenhauer JG (2003) Regression through the origin. *Teaching Statistics* **25**, 76–80. doi:10.1111/1467-9639.00136

Engl HW, Hanke M, Neubauer A (1996) 'Regularization of Inverse Problems.' (Springer-Verlag: New York)

Galgano A, Di Blasi C (2004) Modeling the propagation of drying and decomposition fronts in wood. *Combustion and Flame* **139**, 16–27. doi:10.1016/J.COMBUSTFLAME.2004.07.004

Gardner L, Ng KT (2006) Temperature development in structural stainless steel sections exposed to fire. *Fire Safety Journal* **41**, 185–203. doi:10.1016/J.FIRESAF.2005.11.009

Groetsch CW (1993) 'Inverse Problems in the Mathematical Sciences.' (Friedrich Vieweg and Sohn: Braunschweig, Wiesbaden)

Gutsell SL, Johnson EA (1996) How fire scars are formed: coupling a disturbance process to its ecological effect. *Canadian Journal of Forest Research* **26**, 166–174. doi:10.1139/X26-020

Hansen PC (2001) The L-curve and its use in the numerical treatment of inverse problems. In 'Computational Inverse Problems in Electrocardiology'. pp. 119–142. (WIT Press: Southampton, UK)

Huang C-H, Yeh C-Y (2002) An inverse problem in simultaneous estimating the Biot numbers of heat and moisture transfer for a porous material. *International Journal of Heat and Mass Transfer* **45**, 4643–4653. doi:10.1016/S0017-9310(02)00161-8

Incropera FP, DeWitt DP (2002) 'An Introduction to Heat Transfer.' 4th edn. (Wiley: New York)

Jones JL, Webb BW, Jimenez D, Reardon J, Butler BW (2004) Development of an advanced one-dimensional stem heating model for application in surface fires. *Canadian Journal of Forest Research* **34**, 20–30. doi:10.1139/X03-187

Jones JL, Webb BW, Butler BW, Dickinson MB, Jimenez D, Reardon J, Bova AS (2006) Prediction and measurement of thermally induced cambial tissue necrosis in tree stems. *International Journal of Wildland Fire* **15**, 3–17. doi:10.1071/WF05017

Kim SK, Lee WI (2002) Solution of inverse heat conduction problems using maximum entropy method. *International Journal of Heat and Mass Transfer* **45**, 381–391. doi:10.1016/S0017-9310(01)00155-7

Kötz B, Schaepman M, Morsdorf F, Bowyer P, Ittena K, Allgöwerd B (2004) Radiative transfer modeling within a heterogeneous canopy for estimation of forest fire fuel properties. *Remote Sensing of Environment* **92**, 332–344. doi:10.1016/J.RSE.2004.05.015

Kurpisz K, Nowak AJ (1995) 'Inverse Thermal Problems.' (Computational Mechanics Publications: Southampton, UK)

Lagier GL, Lemonnier H, Coutris N (2004) A numerical solution of the linear multidimensional unsteady inverse heat conduction problem with the boundary element method and the singular value decomposition. *International Journal of Thermal Sciences* **43**, 145–155. doi:10.1016/J.IJTHERMALSCI.2003.06.002

Lesnic D, Elliott L, Ingham DB (1996) Application of the boundary element method to heat conduction problems. *International Journal of Heat and Mass Transfer* **39**, 1503–1517. doi:10.1016/0017-9310(95)00229-4

Lin SM, Chen CK, Yang YT (2004) A modified sequential approach for solving inverse heat conduction problems. *International Journal of Heat and Mass Transfer* **47**, 2669–2680. doi:10.1016/J.IJHEATMASSTRANSFER.2003.11.027

Martin RE (1963) Thermal properties of bark. *Forest Products Journal* **8**, 419–426.

Monde M, Arima H, Liu W, Mitutake Y, Hammad JA (2003) An analytical solution for two-dimensional inverse heat conduction problems using Laplace transform. *International Journal of Heat and Mass Transfer* **46**, 2135–2148. doi:10.1016/S0017-9310(02)00510-0

Nakos JT (2005) Uncertainty analysis of steady-state incident heat flux measurements in hydrocarbon fuel fires. Sandia National Laboratories, Technical Report SAND2005–7144. Available at http://prod.sandia.gov/techlib/access-control.cgi/2005/057144.pdf [Verified 11 August 2009]

Radeloff VC, Mladenoff DJ, Boyce MS (1999) Detecting jack pine budworm defoliation using spectral mixture analysis: separating effects from determinants. *Remote Sensing of Environment* **69**, 156–169. doi:10.1016/S0034-4257(99)00008-5

Roberts DA, Ustin SL, Ogunjemiyo S, Greenberg J, Dobrowski SZ, Chen J, Hinckley TM (2004) Spectral and structural measures of Northwest forest vegetation at leaf to landscape scales. *Ecosystems* **7**, 545–562. doi:10.1007/S10021-004-0144-5

Rubio E, Caselles V, Badenas C (1997) Emissivity measurements of several soils and vegetation types in the 8–14 μm wave band: analysis of two field methods. *Remote Sensing of Environment* **59**, 490–521. doi:10.1016/S0034-4257(96)00123-X

Siau JF (1995) 'Wood: Influence of Moisture on Physical Properties.' (Department of Wood Science and Forest Products, Virginia Polytechnic Institute and State University: Blacksburg, VA)

Shen DK, Fang MX, Luo ZY, Cen KF (2007) Modeling pyrolysis of wet wood under external heat flux. *Fire Safety Journal* **42**, 210–217. doi:10.1016/J.FIRESAF.2006.09.001

Shenefelt JR, Luck R, Taylor RP, Berry JT (2002) Solution to inverse heat conduction problems employing singular value decomposition and model reduction. *International Journal of Heat and Mass Transfer* **45**, 67–74. doi:10.1016/S0017-9310(01)00129-6

van Mantgem P, Schwartz M (2003) Bark heat resistance of small trees in California mixed conifer forests: testing some model assumptions. *Forest Ecology and Management* **178**, 341–352. doi:10.1016/S0378-1127(02)00554-6

Wu L (2003) A parameter choice method for Tikhonov regularization. *Electronic Transactions on Numerical Analysis* **16**, 107–128. Available at http://etna.mcs.kent.edu/vol.16.2003/pp107-128.dir/pp107-128.pdf [Verified 14 September 2009]

Manuscript received 23 August 2007, accepted 2 September 2008